

Time-of-flight modeling of transversal ultrasonic scan of wood

Natalia Yaitskova^{a)} and Jan Willem van de Kuilen^{b)}

Holzforschung München, Technische Universität München, Winzererstraße 45, D-80797, Munich, Germany

(Received 18 December 2013; revised 4 April 2014; accepted 9 April 2014)

Time-of-flight is a time for an ultrasonic pulse to cross a sample. It contains valuable information about the mechanical properties of a material. For the ultrasonic pulse propagating in wood perpendicular to the grain the relation between the time-of-flight and the elastic constants is rather complex due to the strong anisotropy of wood. With the help of some assumptions this relation can be established from the elastic theory. The analytical calculation results in a function which represents a change of time-of-flight when the direction of propagation shifts from the radial to the tangential direction while scanning a board crosswise. The function takes into account the location of the pith and the geometry of the growth rings. The measurement performed on a sample of European spruce confirms the theoretical prediction. © 2014 Acoustical Society of America. [<http://dx.doi.org/10.1121/1.4873519>]

PACS number(s): 43.35.Zc, 43.35.Cg, 43.20.Bi [JDM]

Pages: 3409–3415

I. INTRODUCTION

Ultrasonic testing of wood is a well-established method and it is widely exploited in industry, technology, and science. The velocity of propagation of an ultrasonic wave, the damping, and the polarization are directly related to the mechanical properties of the material in which the wave propagates. The parameters of the wave are used to determine important mechanical characteristics of wood, such as elastic coefficients and density.

There are several applications which require the ultrasonic assessment of wood quality. Most important are testing of the quality of standing trees and to assess the tree's wood quality,¹ determination of wood quality in historical buildings,² and timber grading at sawmills to ensure the supply of appropriate strength graded timber for structural use.³

There are three main methods of ultrasonic non-destructive testing applied for wood assessment: (a) high-resolution imaging, or B-scans, (b) tomography, and (c) longitudinal pitch-catch system. In high-resolution imaging the details of the inner structure of wood are visualized by registering the time of propagation of the signal reflected on acoustical inhomogeneities, i.e., changes of impedance.^{2,4} It is similar to the ultrasonic diagnostics in medicine. In ultrasonic tomography, the inner structure of wood is reconstructed with the use of circular arranged ultrasonic probes, registering the velocity and damping of the ultrasonic wave along the intercrossing paths.^{1,5} In the longitudinal pitch-catch system, the time-of-flight of the ultrasonic pulse is measured in a longitudinal direction along the board.^{3,6} This time-of-flight is related to the speed of sound and hence, to the modulus of elasticity. Unlike two previous methods, this is not an imaging system, because there is only one measurement per board. This measurement is used to grade the wood to determine its further use.

The high resolution ultrasonic imaging and tomography have so far not been proven suitable for the industrial machine grading, which requires processing of 50–150 pieces per minute in order to be economical. Besides, the systems utilizing these techniques are generally costly and unaffordable for small and medium enterprises.

Ultrasound longitudinal grading alone proved not to be very sufficient in increasing the yield in higher strength classes of wood. It should be combined either with visual grading⁷ or with x-ray scanning.⁸ The drawback of the first approach is that it is time-consuming and not fully automated, the second approach poses the problem of cost.

A grading machine must be fast, relatively inexpensive, reliable for the large range of cross sections and wood quality, and preferable fully automated. Transversal ultrasonic scan might be a solution of this nontrivial task. In the prototypes of such machine two types of transducers have been used: dry-contact transducer and air-coupled transducer. In the first approach the transducer's head must be firmly pressed against the surface to provide a good coupling. It can also utilize some special coupling material, such as rubber. The measurements described in the present paper were done using a single point pair transmitter/receiver with a dry-contact. To increase the speed of measurement the dry-contact transducers are usually implemented as arrays and mounted into a roller.^{9,10} In the case of air-coupled transducers^{11,12} there is an air gap between the transducer's head and the material, typically equal to the size of the near-field. The advantage of this approach is that no special coupling or pressure system required and the disadvantage is a low signal-to-noise ratio due to the huge losses caused by the reflection between the air and the wood. So far the air-coupled transducers have been used only on the boards with the thickness no more than 7 mm.

In both schemes, with dry-contact or air-coupled, an ultrasonic pulse propagates in the transversal direction and the time-of-flight is registered at each receiver. The raw data is a two-dimensional (2D) image of the board, where each pixel is the time-of-flight registered for each area on the board (equal to the area of the receiver). Together with the time-of-flight,

^{a)} Author to whom correspondence should be addressed. Electronic mail: yaitskova@hfm.tum.de

^{b)} Also at: Delft University of Technology, Faculty of Civil Engineering and Geosciences, Stewinweg 1, 2628 CN, Delft, Netherlands.

one can also measure attenuation of the wave; in this case the raw data is two 2D images.

Transversal ultrasonic scan combines the principles of the visual grading with an ultrasonic measurement. The measurements must be sensitive to wood defects such as knots, fiber deviation, crack, etc. The present paper studies the physical principle of such imaging. The elastic theory of orthotropic medium allows obtaining a time required for a wave to cross the board. In general, the propagation in question does not happen along the main axes of the wood, so one must handle the case of quasi-longitudinal wave with polarization vector changing along the direction of propagation. Section II recalls the theory of mechanics of the orthotropic medium related to wave propagation phenomenon. This material can be found in any text book on acoustics and in particular, in the books devoted to the acoustics of wood by Bucur.¹³ But, as it is the fundament of the present study, it is necessary to summarize it in Sec. II. Section III calculates the time of propagation across the grains of clear, ideal wooden board. The clear wood is assumed to have no defects; “ideal board” is a board without any fiber deviation, the long side is strictly aligned with the direction of fibers and the structure of the growth rings is perfectly circular. The difference in scanned images between ideal and real wood may serve in the future as one of possible criteria to estimate the quality of wood. The curves are presented for the values for stiffness and density typical for the European spruce. Section IV describes the results of measurement of a sample of spruce and compares them with the theoretical profile.

II. WAVE PROPAGATION IN ORTHOTROPIC MEDIUM

A. Wave equation

The starting point is a linearized three-dimensional equation of motion

$$\rho \ddot{\mathbf{u}} + \nabla \cdot \hat{\sigma} = 0, \quad (1)$$

here ρ is local density, \mathbf{u} is the displacement vector, and $\hat{\sigma}$ is the stress tensor. In general, all of these parameters are functions of space coordinates. The stress tensor $\hat{\sigma}$ is related to the strain tensor $\hat{\varepsilon}$ by the generalized Hooke's law

$$\hat{\sigma} = -\hat{C}\hat{\varepsilon}, \quad (2)$$

where \hat{C} is stiffness tensor, which describes all (linear) mechanical properties of the material. The equation directly uses the Voigt notation: the stiffness tensor has rank 2 (matrix) and the stress and the strain tensors have rank 1 (vectors). Within the frame of the infinitesimal strain theory, assuming the displacements of particles to be much smaller than the characteristic dimension of the body, the strain tensor $\hat{\varepsilon}$ is related to the gradient of the displacement vector \mathbf{u} as

$$\hat{\varepsilon} = \frac{1}{2} [(\nabla \mathbf{u})^T + (\nabla \mathbf{u})], \quad \|\mathbf{u}\| \ll 1, \quad \|\nabla \mathbf{u}\| \ll 1. \quad (3)$$

Combining Eq. (1) with Eqs. (2) and (3) one notices that Eq. (1) relates the second time derivative and the second

space derivative of \mathbf{u} , i.e., it represents a wave equation for the displacement vector. In order to illustrate it, let us consider a simple case: when the motion is one-dimensional, all tensors included in the equations are scalars, and the stiffness tensor, or Young's modulus, is invariant in space. In this case, it is easy to show that Eq. (1) reduces to $\rho \ddot{u} - C(d^2u/dx^2) = 0$, the one-dimensional wave equation.

In further analysis, the following factors are not considered: (1) the attenuation by the medium, i.e., absorption and scattering; (2) the local changes of the stiffness tensor, $\|\nabla \cdot \hat{C}\| \ll 1$; and (3) the internal reflections (echoes), diffraction, and interference.

B. Stiffness tensor for orthotropic material

The model of a clear, ideal board assumes the following: the fibers are aligned strictly parallel to the long side of the cut, the annual rings have a perfect circular geometry, no knots are present, nor are cracks, or any other type of defects. For a given stiffness tensor and density this ideal board possesses the maximal mechanical properties (for example, a bending strength). Any deviation from the ideal shape: grain not parallel to the long side (fiber deviation), local change of the density (reaction wood), knots, cracks, etc. will influence the mechanical properties. Any regular changes of the density and the stiffness tensor, as for instance between juvenile and mature wood or between the annual rings, can be included into the model of ideal wood. Also, possible non-circular, elliptical shapes of the rings can be included into the model. Although, for the sake of simplicity the final calculation does not take these features into account, Sec. III A shows how this can be done.

It is helpful to introduce two systems of coordinates (Fig. 1): the global one (XYZ), related to the shape of the board with the center of coordinates in pith, and the local one (LTR), related to the wood structure. For any point, the axes of the local system of coordinate are parallel to the grain (L), tangential to the annual rings (T), and perpendicular to the annual rings and to the grains (R). The LTR system of coordinates is transformed into the XYZ system of coordinates by a rotation matrix: If the long side of the board is not

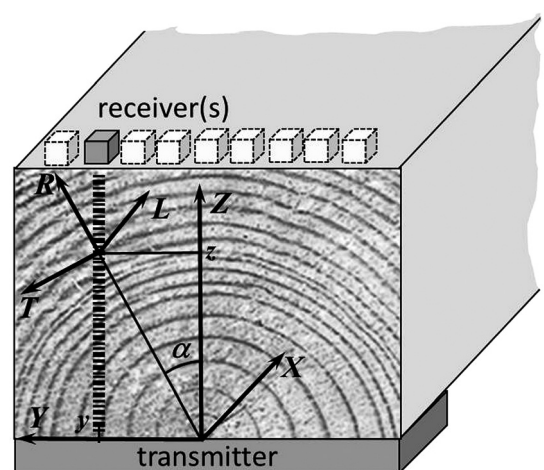


FIG. 1. Geometry of a board: XYZ -coordinate system is related to the sides of the board; LTR -system is related to the main axes of the wood.

parallel to the grain, the rotation includes three angles, if the long side of the board is parallel to the grain (ideal wood), the rotation is in the YZ -plane only and a transformation matrix \hat{a} includes only one angle α ,

$$\hat{a} = \begin{bmatrix} 1 & 0 & 0 \\ 0 & \cos(\alpha) & -\sin(\alpha) \\ 0 & \sin(\alpha) & \cos(\alpha) \end{bmatrix}. \quad (4)$$

If one also needs to include into the model the non-parallelism between the direction of the grain and the surfaces of the board (so-called fiber deviation), the transformation matrix will be a multiplication of three sequential rotations: by angle α around OX , by angle θ around OY , and by angle φ around OZ .

Wood is an anisotropic material, which means that the mechanical properties are different in L , T , and R directions, but assuming orthotropic behavior can be justified for most applications.^{14,15} It means that the stiffness tensor \hat{C} in the LTR system of coordinates is symmetric and sparse,

$$\hat{C} = \begin{bmatrix} C_{11} & C_{12} & C_{13} & 0 & 0 & 0 \\ C_{12} & C_{22} & C_{23} & 0 & 0 & 0 \\ C_{13} & C_{23} & C_{33} & 0 & 0 & 0 \\ 0 & 0 & 0 & C_{44} & 0 & 0 \\ 0 & 0 & 0 & 0 & C_{55} & 0 \\ 0 & 0 & 0 & 0 & 0 & C_{66} \end{bmatrix}. \quad (5)$$

$$\hat{M} = \begin{bmatrix} 1 & 0 & 0 & 0 & 0 & 0 \\ 0 & \cos^2(\alpha) & \sin^2(\alpha) & -\sin(2\alpha) & 0 & 0 \\ 0 & \sin^2(\alpha) & \cos^2(\alpha) & \sin(2\alpha) & 0 & 0 \\ 0 & \frac{1}{2}\sin(2\alpha) & -\frac{1}{2}\sin(2\alpha) & \cos(2\alpha) & 0 & 0 \\ 0 & 0 & 0 & 0 & \cos(\alpha) & \sin(\alpha) \\ 0 & 0 & 0 & 0 & -\sin(\alpha) & \cos(\alpha) \end{bmatrix}. \quad (9)$$

After the rotation, some zeros of the matrix \hat{C} become non-zero. More complex rotation by three angles removes all zeros from the stiffness tensor.

The stiffness tensor and the density determine the properties of the acoustic wave, its speed and polarization. To measure the stiffness tensor in wood is an important issue; nevertheless it is not a trivial task. There are many papers concerning the measurements of all nine constants of the stiffness tensor using ultrasonic techniques.^{16–19} For this study it is assumed that the stiffness tensor is known.

C. Plane-wave solution

The standard development is to look for the solution of the Eq. (1) in the form of a monochromatic plane wave

The elements of the tensor are related to the elastic constants as

$$\begin{aligned} C_{11} &= q(-1 + \nu_{TR}\nu_{RT})E_L, & C_{12} &= -q(\nu_{TL} + \nu_{TR}\nu_{RL})E_L, \\ C_{13} &= -q(\nu_{RL} + \nu_{TL}\nu_{RT})E_L, \\ C_{22} &= q(-1 + \nu_{LR}\nu_{RL})E_T, & C_{23} &= -q(\nu_{RT} + \nu_{LT}\nu_{RL})E_T, \\ C_{33} &= q(-1 + \nu_{LT}\nu_{TL})E_R, \\ C_{44} &= 2G_{TR}, & C_{55} &= 2G_{LR}, & C_{66} &= 2G_{LT}, \end{aligned} \quad (6)$$

and parameter q is

$$q = (-1 + \nu_{LT}\nu_{TL} + \nu_{LR}\nu_{RL} + \nu_{TR}\nu_{RT} + \nu_{TR}\nu_{LT}\nu_{RL} + \nu_{LR}\nu_{TL}\nu_{RT})^{-1}. \quad (7)$$

The elastic constants are E_L, E_T, E_R —elastic moduli in L, T , and R directions; G_{TR}, G_{LR}, G_{LT} —shear moduli; and $\nu_{LT}, \nu_{TL}, \dots$ —Poisson ratios.

To calculate the stiffness tensor in the XYZ system of coordinates the transformation for the second-rank tensor must be applied,

$$\hat{C}' = \hat{M}\hat{C}\hat{M}^T, \quad (8)$$

where the elements of the Bond transformation matrix \hat{M} are the algebraic expressions of the elements of the transformation matrix \hat{a} . Again, rotation around only one axis is relatively simple,

$$\mathbf{u}(\mathbf{x}, t) = \mathbf{p} \exp(i\omega t - i\mathbf{k} \cdot \mathbf{x}), \quad (10)$$

where $\mathbf{x} = (x, y, z)$ is the three-dimensional position vector, t is the time, \mathbf{p} is the polarization vector, indicating the direction of oscillations, k is the wave number, \mathbf{d} is the propagation unit vector, ω is the frequency of oscillations. The speed of sound is $v = \omega/k$.

The next step is to substitute Eq. (10) into the wave equation Eq. (1), where the stiffness tensor \hat{C} must be replaced by the rotated stiffness tensor \hat{C}' . By doing so, one obtains a system of linear equations for the polarization vector \mathbf{p} , called Christoffel's equations,

$$(\hat{\Gamma} - \rho v^2 \hat{I})\mathbf{p} = 0, \quad (11)$$

where \hat{I} is a diagonal unit-matrix, while the elements of the Christoffel's matrix $\hat{\Gamma}$ are linear combinations of the

elements of the matrix \hat{C} , rotation angles, and the components of the propagation vector \mathbf{d} . The general solution involves the eigenvector problem of the Christoffel's matrix $\hat{\Gamma}$. In the chosen setup (Fig. 1), the wave propagates along the Z-direction and $\mathbf{d} = (0, 0, 1)$. The eigenvector problem of the Christoffel's matrix $\hat{\Gamma}$ gives three solutions. It means that vibrations propagating in Z-direction can be decomposed in three waves:¹³ quasi-longitudinal, quasi-shear, and pure shear. Three waves correspond to three different eigenvalues, i.e., each of them propagates with a different speed. The ultrasonic systems mentioned in the Sec. I usually work with the quasi-longitudinal wave. Although the quasi-shear wave also has a non-zero projection of the vibration on the Z-axis, but this component is small. Besides, the quasi-shear wave propagates with a speed two to three times less than that of the quasi-longitudinal wave and the two components can be distinguished.

The eigenvalue for the quasi-longitudinal wave is

$$2\rho\nu^2 = \Gamma_{33} + \Gamma_{22} + \sqrt{(\Gamma_{33} - \Gamma_{22})^2 + 4\Gamma_{23}^2}. \quad (12)$$

As the stiffness matrix is supposed to be known, the free parameter here is angle α between the direction of propagation and the radial axis of wood. It is convenient to normalize ν to the speed in tangential direction, ν_T ,

$$\nu_T = \nu(\alpha = 0) = \sqrt{C_{22}/\rho} \quad (13)$$

and re-write Eq. (12) with respect to the angle α for the normalized speed,

$$\left(\frac{\nu}{\nu_T}\right)^2 = \kappa_0 + \kappa_1 \cos^2(\alpha) + \sqrt{(1 - \kappa_0)^2 - \kappa_2 \cos^2(\alpha) + \kappa_3 \cos^4(\alpha)}, \quad (14)$$

where $\kappa_0, \dots, \kappa_3$ are coefficients, calculated from the stiffness matrix

$$\begin{aligned} \kappa_0 &= \frac{C_{22} + C_{44}}{2C_{22}}, & \kappa_1 &= \frac{C_{33} - C_{22}}{2C_{22}}, \\ \kappa_2 &= \frac{1}{2C_{22}^2} (C_{22}^2 + C_{22}C_{33} - 3C_{22}C_{44} - 2C_{23}^2 \\ &\quad - 4C_{23}C_{44} - C_{33}C_{44}), \\ \kappa_3 &= \frac{1}{4C_{22}^2} (C_{22} + 2C_{23} + C_{33}) \\ &\quad \times (C_{22} + C_{33} - 4C_{44} - 2C_{23}). \end{aligned} \quad (15)$$

Equation (14) relates the speed of the quasi-longitudinal wave to the angle between the direction of propagation and the radial axis of wood. When $\alpha = 0$ direction of propagation coincides with the radial direction and $(\nu/\nu_T)^2 = C_{33}/C_{22}$. In the opposite case, when $\alpha = \pi/2$ direction of the propagation coincides with the tangential direction and $(\nu/\nu_T)^2 = 1$. Knowledge of the speed of sound for the arbitrary

orientation between the radial and the tangential directions is sufficient to now calculate the time-of-flight.

III. TIME-OF-FLIGHT MODELING

A. Wave propagation perpendicular to the grain

While the wave propagates along OZ the angle α changes (Fig. 1) as

$$\cos(\alpha) = \frac{z}{R}, \quad (16)$$

where $R = \sqrt{z^2 + y^2}$ is the distance from the current position to the pith. Representing the speed as $\nu = dz/dt$ yields to the following expression for the total time-of-flight:

$$\begin{aligned} t(y) &= \int_{z_1}^{z_2} \frac{dz}{\nu(z)} = \int_{z_1}^{z_2} \nu_T^{-1}(R) \left[\kappa_0(R) + \kappa_1(R) \frac{z^2}{R^2} \right. \\ &\quad \left. + \sqrt{[1 - \kappa_0(R)]^2 - \kappa_2(R) \frac{z^2}{R^2} + \kappa_3(R) \frac{z^4}{R^4}} \right]^{-1/2} dz, \end{aligned} \quad (17)$$

where z_1 and z_2 are the coordinate of the transmitter and receiver with respect to the pith. (In Fig. 1 $z_1 = 0$ and z_2 equals to the thickness of the board.)

In general, parameters ν_T , and $\kappa_0 \dots \kappa_3$ are functions of R . The gradual change of the density and stiffness between the juvenile and mature wood can be taken into account by including some models for these parameters. In a simplified calculation these parameters are assumed to be invariable. Some mathematical re-arrangement yields in the following result for time-of-flight:

$$t(y) = \nu_T^{-1} \left[z_2 g\left(\frac{y}{z_2}\right) - z_1 g\left(\frac{y}{z_1}\right) \right], \quad (18)$$

where

$$\begin{aligned} g(\gamma) &= \gamma \int_0^{\gamma^{-1}} \{ \kappa_0 + \kappa_1(1 + u^{-2})^{-1} \\ &\quad + [(1 - \kappa_0)^2 - \kappa_2(1 + u^{-2})^{-1} \\ &\quad + \kappa_3(1 + u^{-2})^{-2}]^{1/2} \}^{-1/2} du. \end{aligned} \quad (19)$$

This integral can be calculated either numerically or with the help of any symbolic calculation software, for example MATHEMATICA or MAPLE. To plot function $g(\gamma)$ one must choose some values for the parameters $\kappa_0, \dots, \kappa_3$, which are related to the elastic constants. Of course, the values of these parameters vary between and within the species; they also depend on the growth region, the wood moisture content, the density, and so on. The following calculations are done for the European spruce with the density in a range of 350–480 kg/m³, moisture content of 8%–10%, based on the values for the elastic constants reported by Hearmon.²⁰ Table I presents the parameters $\kappa_0, \dots, \kappa_3$ together with the elastic coefficients upon which they depend according to

TABLE I. Parameters, related to the calculation of time-of-flight for spruce. Units: kg/m^3 , GPa, km/s. Coefficients $\nu_{RT}, \dots, \nu_{LT}$ and $\kappa_0, \dots, \kappa_3$ are unitless.

ρ	E_R	E_T	G_{TR}	ν_{RT}	ν_{RL}	ν_{TR}	ν_{TL}	ν_{LR}	ν_{LT}	κ_0	κ_1	κ_2	κ_3	ν_T
370	0.73	0.41	0.022	0.57	0.031	0.29	0.013	0.44	0.56	0.54	0.39	0.73	1.25	1.16
390	0.71	0.43	0.023	0.51	0.03	0.31	0.025	0.38	0.51	0.54	0.32	0.74	1.14	1.16
430	0.89	0.48	0.032	0.56	0.03	0.3	0.019	0.45	0.54	0.55	0.43	0.7	1.27	1.17
440	0.69	0.39	0.036	0.47	0.028	0.25	0.013	0.44	0.38	0.58	0.39	0.61	1.09	1.01

Eqs. (6), (7), and (15), as well as the tangential speed of sound. Function $g(\gamma)$ is plotted in Fig. 2.

Function $g(\gamma)$ is symmetric around zero, achieves a minimum when $\gamma = 0$: $g_0 = \sqrt{C_{22}/C_{33}}$, and saturates to unity at large γ . The minimum corresponds to the minimal time-of-flight in the radial direction

$$t_R = \nu_T^{-1}(z_2 - z_1)\sqrt{C_{22}/C_{33}}. \quad (20)$$

The saturation level corresponds to the maximal time-of-flight in the tangential direction

$$t_T = \nu_T^{-1}(z_2 - z_1). \quad (21)$$

It is more practical to use a more simple function, rather than directly Eq. (19). The function $g(\gamma)$ can be substituted by a polynomial ratio

$$g_{fit}(\gamma) = \frac{g_0 + a_1|\gamma| + a_2|\gamma|^3}{1 + b_1|\gamma| + a_2|\gamma|^3}, \quad (22)$$

where $g_0 = \sqrt{C_{22}/C_{33}}$ and a_1, a_2 , and b_1 are the fitting coefficients. This polynomial ratio possesses the same properties as the function $g(\gamma)$: it has a minimum equal to g_0 at zero, saturates to unity at large argument, and has a slight local maximum around $\gamma = 1.4-1.8$.

Table II gives the fitting coefficients for the four densities of spruce listed in the Table I. For these four cases a chi-square difference between functions $g(\gamma)$ and $g_{fit}(\gamma)$ is about 10^{-7} and on the plot the initial and fitted curves are undistinguishable.

B. Influence of position of pith

According to Eq. (18) the time-of-flight strongly depends on the position of pith (the center of coordinated of XYZ-system). This influence can be followed by varying the low border of the board (parameter z_1) and keeping the total

TABLE II. Fitting coefficients the function $g(\gamma)$ for different densities of spruce. Units of density: kg/m^3 ; other parameters are unitless.

ρ	g_0	a_1	a_2	b_1
370	0.748	1.41	2.22	1.16
390	0.780	1.38	2.28	1.10
430	0.733	1.43	2.20	1.20
440	0.749	1.44	2.27	1.21

width of a board fixed. Curves on Fig. 3 are calculated for four cases: $z_1 = -d/2$, when the pith is located within the board in the center; $z_1 = 0$, when pith is at the edge of the board; $z_1 = d/2$; and $z_1 = d$, when the pith is located not within the board, but at 60 mm outside of it. The thickness of the board $d = z_2 - z_1$ in all cases is equal to 60 mm. The sharpest curve corresponds to the case when the pith is located in the center of the board. While the pith is moving further and further from the board the curvature of the annular rings decreases and the direction of propagation approaches the radial direction; the time-of-flight curve descends and eventually becomes a horizontal line with $t = t_R$.

IV. MEASUREMENT OF SPRUCE

The theoretical prediction of time-of-flight is verified by the measurement on a sample of European spruce. The average density of the sample is 405 kg/m^3 , moisture content 9%, thickness of the board $d = 62 \text{ mm}$, width 103 mm. To time-of-flight was measured with a PUNDIT Mark V ultrasonic device using Exponential Probe receiving and transmitting transducers. The central frequency is 54 kHz. The diameter of the probe's tip is 6 mm and is flat for the transmitter and round-shaped for the receiver. As the size of an aperture is much less than a wavelength (around 30 mm) the propagation can be regarded as "point to point." According to Huygens-Fresnel principle the point-to-point propagation can be calculated using a plane-wave model.

Figure 4 shows a photograph of the end of the board with the structure of the growth rings. The line of the scan is 20 mm from the end. For this sample pith is not included in

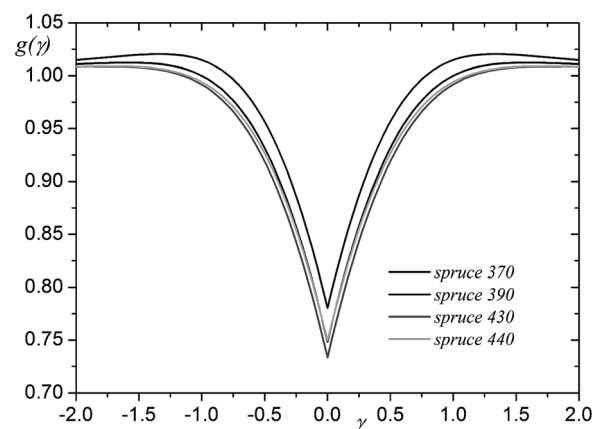


FIG. 2. Function $g(\gamma)$ for different densities of spruce.

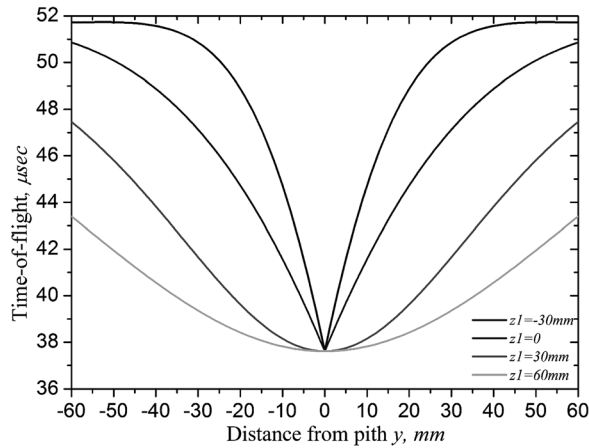


FIG. 3. Time-of-flight for different positions of the pith. Spruce density 430 kg/m^3 , board thickness 60 mm . Parameters of the curves are in the Tables I and II.

the wood, but is estimated to be located 8 mm below the cut. Figure 5 shows the results of the scan: time-of-flight with 2 mm sampling. The $25 \mu\text{s}$ calibration time was subtracted from each measurement. The theoretical curve is fitted to the data. The fitted parameters are not so different from the ones in the Table II: $g_0 = 0.75$, $a_1 = 1.47$, $a_2 = 2.20$, $b_1 = 1.15$, $\nu_T = 1.17 \text{ km/c}$.

There are two areas in which the measurements fall away from the theoretical curve: from -60 to -40 and from 20 to 30 mm . These areas correspond to the defects, which can be seen on the photograph as a deviation of the growth-ring structure from the circular geometry. The area from 20 to 30 mm corresponds to a knot; area from -60 to -40 mm is compressed wood. If one subtracts the fitted curve from the measurement, the result will contain the information about the size and location of the defects and it can be used afterward for an automatic recognition and classification of the defects.

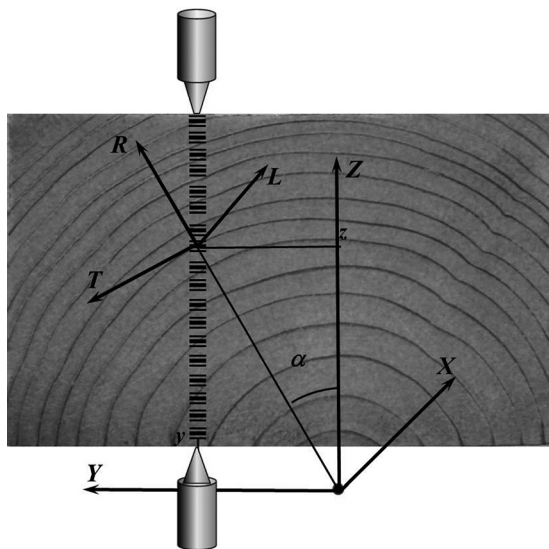


FIG. 4. Configuration of the measurement. A photograph of the end of the sample shows the geometry of the growth rings. Pith is located at 8 mm below the lower border of the board.

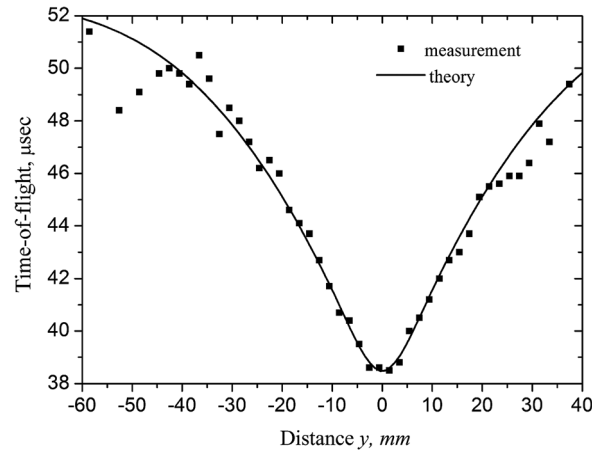


FIG. 5. Results of measurement and the theoretical curve with fitted parameters: $g_0 = 0.75$, $a_1 = 1.47$, $a_2 = 2.20$, $b_1 = 1.15$, $\nu_T = 1.17 \text{ km/c}$.

V. CONCLUSION

When the direction of wave propagation changes from the radial (R) to the tangential (T) direction, the profile of time-of-flight (RT -profile) has a V-like shape, and depends on the elastic coefficients, density, and position of pith. This profile was calculated directly from the theory of wave propagation and fitted by the polynomial ratio which can be used to avoid analytical integration and implementation of any special functions.

The examples of calculations were done for the most favorable case of dry mature spruce, when the difference of elastic parameters in different directions is large. The contrast of the RT -profile (the difference in time-of-flight between the radial and the tangential directions) is $13 \mu\text{s}$ for 62 mm thickness. With the moisture content increasing, the contrast of the RT -profile will decrease. A similar effect is associated with the juvenile wood: In juvenile wood the difference between C_{22} and C_{33} coefficients is small, and so is the difference in the acoustic speed in R and T directions. The RT -profile will be more flat and shallow in the middle if one takes into account the juvenile part of the board.

This paper concentrates only on the case of clear ideal wood without defects. The defects (essentially, knots) can be detected as deviations of the measurements from the ideal RT -profile. In order to do that one has to define the location of the pith for each position along the board, fit the RT -profile and subtract the RT -profile from the measured data. The resulting image will contain only information about the defects and can be further treated to recognize the defects, represent, and quantify them.

The theory described in this paper, can be further used to model the time-of-flight through a knot. The simplest approach is to consider a knot as an area where the LRT system of coordinate is substituted by the RTL system of coordinate with some increase of a density. One can estimate the sensitivity of knots detection by considering different geometries and locations of this area.

ACKNOWLEDGMENTS

This study is accomplished in the Framework Programme 7, project WoodSonic "A cost-efficient, automated, machine

strength grading system for sawn timber,” Grant Agreement Number 315351.

- ¹V. Bucur, “Ultrasonic techniques for nondestructive testing of standing trees,” *Ultrasonics* **43**(4), 237–239 (2005).
- ²A. Hasenstab, C. Rieck, B. Hillemeier, and M. Krause, “Use of low frequency ultrasound echo technique to determine cavities in wooden constructions,” *Proc. International Symposium Non-Destructive Testing in Civil Engineering*, Berlin (September 16–19, 2003), P51–P59.
- ³J.-L. Sandoz, “Grading of construction timber by ultrasound,” *Wood Sci. Technol.* **23**, 95–108 (1989).
- ⁴A. Hasenstab and M. Krause, “Defect localization in wood with low frequency Ultrasonic Echo Technique,” *Proc. 14th International Symposium on Nondestructive Testing of Wood*, Hannover, Germany (May 2–4, 2005), pp. 211–214.
- ⁵L. Brancheriau, P. Lasaygues, E. Debieu, and J.-P. Lefebvre, “Ultrasonic tomography of green wood using a non-parametric imaging algorithm with reflected waves,” *Ann. For. Sci.* **65**, 712–719 (2008).
- ⁶G. Ravenshorst and J. W. van de Kuilen, “An innovative species independent strength grading model,” *Proc. 9th World Conference in Timber Engineering*, Portland, OR (August 6–10, 2006), pp. 1–8.
- ⁷J. W. van de Kuilen, M. Togni, M. Moschi, and A. Ceccotti, “Strength data of Italian Red spruce (*Picea abies*),” *Proc. International Conference on Probabilistic Models in Timber Engineering*, Arcachon, France (September 8–9, 2005), pp. 135–145.
- ⁸A. Salmi, A. Meriläinen, M. Torkkeli, M. Peura, J. Haapalainen, E. Hægström, and R. Serimaa, “Microelasticity in wood using x-ray diffraction and ultrasound,” *Proc. International Congress on Ultrasonics*, Vienna, Austria (April 9–13, 2007), pp. 54–57.
- ⁹M. Kabir, D. Schmoldt, and M. Schafer, “Roller-transducer scanners of wooden pallet parts for defect detection,” *AIP Conf. Proc.* **557**, 1218–1228 (2001).
- ¹⁰M. Kabir, D. Schmoldt, and M. Schafer, “Time domain ultrasonic signal characterization for defects in thin unsurfaced hardwood lumber,” *Wood Fiber Sci.* **34**, 165–182 (2002).
- ¹¹B. Marchetti, R. Munaretto, G. Revel, and E. Tomasini, “Non-contact ultrasonic sensor for density measurement and defect detection on wood,” *Proc. 16th World Conference on Nondestructive Testing* (2004), pp. 14–21.
- ¹²S.-H. Kee and J. Zhu, “Using air-coupled sensors to determine the depth of a surface-breaking crack in concrete,” *J. Acoust. Soc. Am.* **127**, 1279–1287 (2010).
- ¹³V. Bucur, *Acoustics of Wood* (CRC Press, Boca Raton, FL, 1995), Chaps. 4 and 5, pp. 35–117.
- ¹⁴R. Schumacher, “Compliances of wood for violin top plates,” *J. Acoust. Soc. Am.* **84**, 1223–1235 (1988).
- ¹⁵A. Romano, J. Bucaro, and S. Dey, “Defect detection and localization in orthotropic wood slabs by inversion of dynamic surface displacements,” *J. Acoust. Soc. Am.* **124**, 918–925 (2008).
- ¹⁶V. Bucur and R. R. Archer, “Elastic constants for wood by an ultrasonic method,” *Wood Sci. Technol.* **18**, 255–265 (1984).
- ¹⁷M. E. McIntyre and J. Woodhouse, “On the measuring wood properties. Part 3,” *J. Catgut Acoust. Soc.* **45**, 14–23 (1986).
- ¹⁸R. Longo, T. Delaunay, D. Laux, M. El Mouridi, O. Arnould, and E. Le Clézio, “Wood elastic characterization from a single sample by resonant ultrasound spectroscopy,” *Ultrasonics* **52**, 971–974 (2012).
- ¹⁹J. Ditre, “On the determination of the elastic moduli of anisotropic media from limited acoustical data,” *J. Acoust. Soc. Am.* **95**, 1761–1767 (1994).
- ²⁰R. Hearmon, “The elasticity of wood and plywood,” *Nature* **162**, 826 (1948).